

Article

Numerical Study of the Riverine Microplastic Distribution in the Arctic Ocean

Elena Golubeva *  and Marina Gradova

Institute of Computational Mathematics and Mathematical Geophysics, Siberian Branch of the Russian Academy of Sciences (SB RAS), 630090 Novosibirsk, Russia; gradova.ma.22@gmail.com

* Correspondence: e.golubeva.nsk@gmail.com

Abstract: Marine plastic pollution is currently one of the most serious environmental threats. In this study, based on scenario calculations for a five-year period, we analyzed the possible spread of microplastics carried by Siberian rivers to the Kara Sea shelf. The Lagrangian particle model used daily data from 3D numerical modeling to simulate microplastic transport by ocean currents and sea ice drift. The results of a series of scenario calculations show how the distribution of particles and their subsequent deposition depend on their type (density), size, processes of freezing into the ice, and biofouling (accumulation of microorganisms). The crucial influence of the effects of microplastic embedding in sea ice and particle biofouling on the trajectories of floating particles and their deposition on the seafloor is highlighted. The transport of light particles of microplastics from Siberian rivers by ice can contribute to the pollution of the Barents Sea, in addition to their more active outflow through the Fram Strait. Biofouling is a driver of microplastic deposition on the shelf bottom or transport along the continental slope in a cyclonic direction following the trajectory of the Atlantic waters.

Keywords: microplastic pollution of the polar waters; numerical modeling; Arctic Ocean; Arctic rivers



Citation: Golubeva, E.; Gradova, M. Numerical Study of the Riverine Microplastic Distribution in the Arctic Ocean. *Water* **2024**, *16*, 441. <https://doi.org/10.3390/w16030441>

Academic Editor: Yuqiang Tao

Received: 27 December 2023

Revised: 19 January 2024

Accepted: 25 January 2024

Published: 29 January 2024



Copyright: © 2024 by the authors. Licensee MDPI, Basel, Switzerland. This article is an open access article distributed under the terms and conditions of the Creative Commons Attribution (CC BY) license (<https://creativecommons.org/licenses/by/4.0/>).

1. Introduction

Plastic pollution of the ocean is one of the most serious environmental threats these days. The global load of plastic on the open ocean surface was estimated to be on the order of tens of thousands of tons [1]. In the environment, due to exposure to sunlight and waves, freezing in the polar regions, mechanical abrasion plastic debris gradually crumble [2]. Breaking down, it forms a huge amount of tiny particles, size < 5 mm, called microplastics [3], that pose the greatest danger to the environment. Floating low-density microplastic (MP) particles are perceived by living organisms as a food source, which is a serious risk to them and can lead to their death. Hundreds of publications have documented the impact of plastic debris on the marine ecosystem (e.g., [4–9]). In addition, the physical and chemical properties of microplastics contribute to the adsorption of contaminants on the surface of particles. Moving up the food chain, microplastics and associated contaminants can enter the human body from seafood [7,8] and affect human health.

Measurement data indicate that microplastics are found in different regions of the world's oceans, from equatorial to polar regions, from the surface to sediment layer [10]. Although assessing pollution transport in Arctic waters is challenging due to the inaccessibility of the region and the lack of permanent observations, plastic pollution has been detected in sea ice [11–14], water masses [15–18], deep-sea sediments [19,20], and in ecosystems [5,9,21]. In addition to local sources (fishery, marine industrial activities, and wastewater), significant sources of plastic include remote regions at lower latitudes, from which pollution is transferred to the Arctic by ocean currents, atmospheric flows, and rivers. It is estimated that 0.013 to 25 million metric tons of micro(nano)plastics can be transported through the marine atmosphere and deposited in the ocean each year [22]. Observations

show that a significant portion of plastic enters the Arctic from the North Atlantic [15,17] and the North Pacific [11,20,23]. As a result of the analysis of water samples in the Eurasian basin [15], two different sources of microplastics were detected, namely inflow from the North Atlantic and discharges from the Great Siberian Rivers (Figure 1). With huge catchment areas, Arctic rivers cross the territory of large cities and industrial and agricultural areas and receive wastewater of unknown purity [24]. The amount of debris in the Siberian shelf seas indicates the low contribution of rivers in autumn [25], but massive river discharges in late spring or summer make potentially significant impacts.

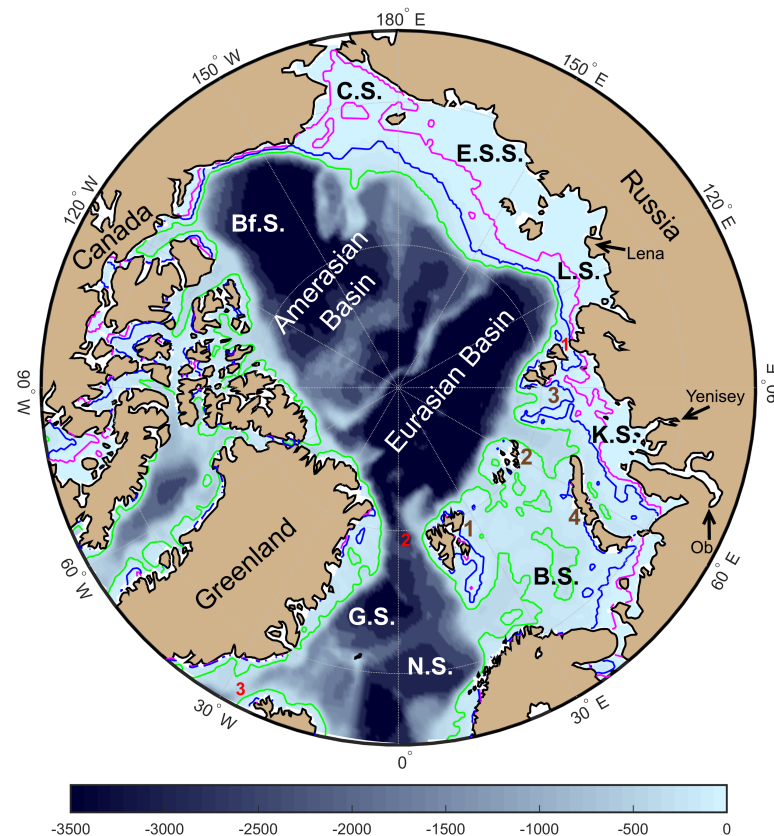


Figure 1. The map of Arctic Ocean bathymetry; magenta, blue, and green lines show the depths of 30, 75, and 300 m. Here, G.S. — Greenland Sea, N.S.—Norwegian Sea, B.S.—Barents Sea, K.S.—Kara Sea, L.S.—Laptev Sea, E.S.S.—East Siberian Sea, C.S.—Chukchi Sea; Bf.S.—Beaufort Sea; brown numbers denote archipelagos: 1—Spitsbergen, 2—Franz Josef Land, 3—Northern Land; red numbers denote straits: 1—Vilkitsky Strait, 2—Fram Strait, 3—Denmark Strait.

Model estimates of the amount of plastic entering the ocean with river water [26] were based on analyses of population density and the quality of plastic waste disposal systems in the catchment area. Among the most polluted rivers in the polar region (Figure 2), only the Ob and Yenisey Rivers flow directly into the Arctic shelf (Figure 1). Based on these estimates, their contribution to the total riverine microplastic load in the polar region equals 46%. The total microplastic influx from the other Arctic rivers not included in this diagram was about 0.2% [26]. Due to the sparse population and limited data on the Lena River, the estimate of riverine plastic input to the Laptev Sea is more than 5000 times lower than in the Kara Sea.

The analysis of observational data describing the concentration of plastic in the marine environment is accompanied by the consideration of a wide range of physical and chemical–biological processes affecting its distribution in the ocean (see [27] for review). There are a number of physical processes that could determine the pathways and fate

of microplastics in the marine environment. Here, we highlight some of them that we are investigating.

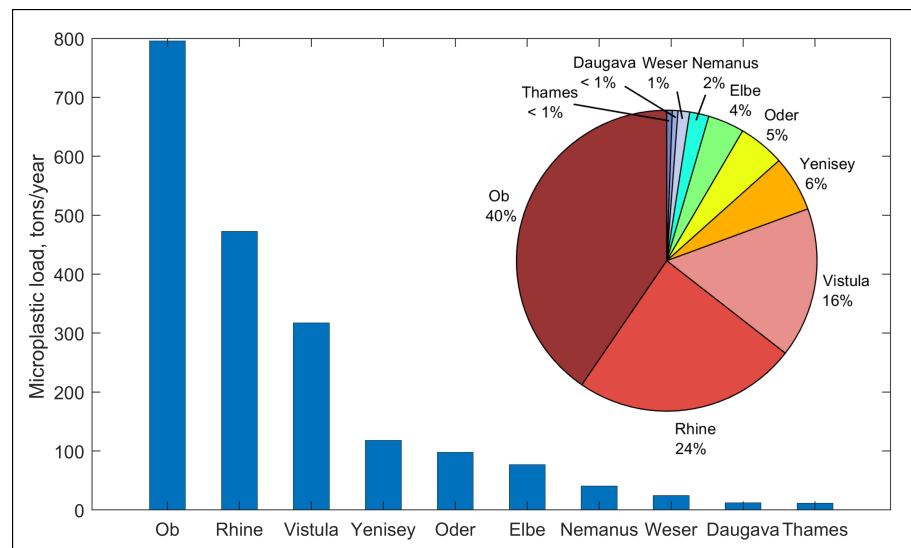


Figure 2. Microplastic load from polar rivers to the ocean waters. The graph was constructed using model estimates [26] based on analyses of population density and the quality of plastic waste disposal systems in the catchment area (refer to [26] Supporting Information). The circle diagram shows the percentage of the microplastic load in each river.

Processes associated with ocean dynamics facilitate the transport of particles over long distances from the original source of pollution. The oceanic pathways followed by the floating debris could be explored using a surface transport model based on data from the Global Drifter Program [27]. Constantly improving numerical models of ocean circulation make it possible to calculate the velocity of currents on regional and global scales.

The difference in the densities of particles and sea water determines the intensity of vertical displacement of the particles, affecting their ability to remain buoyant or to sink into the deeper layers, settling on the seafloor [19]. The presence of particles in the marine environment is accompanied by a concentration of organisms on their surface (biofouling), affecting their buoyancy. Many field studies have shown that the accumulation of biomass, often visually observed on samples, is one of the main mechanisms for changing the chemical and physical properties that can influence the vertical transport of the plastic particles in the water column (e.g., [28–31]).

While in polar regions, microplastic particles become embedded in sea ice and move with its drift, which might be different from the current system of the surface layer. Observations revealed that the amount of MP in Arctic sea ice is extremely high, and, therefore, sea ice can be considered to be a temporary sink for MP [11–14]. The presence of microplastics in sea ice can have a feedback effect on sea ice melting by increasing the albedo effect and changing both ice permeability and solar radiation absorption [32]. Currently, little is known about the behavior of microplastics at the interface of seawater and ice, in particular about the mechanisms of particle entrapment into the ice and release with saline brine back into the ocean and others. A variety of physical processes underlie the interaction of ice and plastic particles [27,33]. To understand this process, a number of laboratory studies have attempted to determine the percentage of plastic particles freezing into the ice [34–36].

An increasing number of publications on microplastics in the marine environment include not only an observational analysis but also works based on numerical modeling. Despite the shortcomings of the numerical approach noted in the review [27], the method of numerical modeling enables the simulation of the transport of microplastics in different areas of the World Ocean and makes it possible to trace the trajectory of particles, determine areas of their accumulation, and to study the sensitivity of the results to parameterization

of physical and biological processes. Currently, similar research for the Arctic Ocean is limited [37–39].

The aim of this study was to clarify the most critical physical processes influencing the transport and distribution of microplastics in the Arctic waters. To solve this problem, we proposed (Section 2) to combine a three-dimensional Lagrangian model of particle transport in marine waters with some parameterizations of physical and biological processes, namely the calculation of particle sinking/rising velocity based on the density difference between microplastics and seawater, and MP particle size; the increasing MP particle density due to biofouling processes; the freezing of floating MPs in sea ice; and their release during ice melt.

In Section 3, we suggested a series of numerical experiments aimed at investigating the sensitivity of MP distribution to account for the above processes. The source of the MPs was considered to be the waters of two major Siberian rivers, the Ob and the Yenisey, because we can set the intensity of the MP influx to the Arctic shelf based on model estimates [26].

The results of a series of 3D numerical simulations (Section 4) show the influence of particle size, particle type (density), and physical and biological processes (freezing into ice and biofouling) on the propagation path of MP particles and their subsequent deposition both on the shelf and beyond. Our findings and some unresolved tasks are discussed in Sections 4 and 5.

2. Data and Methods

2.1. Method of Numerical Simulation of the Arctic Ocean and Sea Ice State

Large-scale ocean circulation is the most powerful way to transport MP particles from estuaries to deep-sea regions. Numerical simulations of the Arctic Ocean circulation, sea ice, and water mass variability were carried out using the three-dimensional numerical ocean and sea ice model SibCIOM (Siberian coupled ice–ocean model) [40,41]. The ocean model is based on Reynolds-averaged primitive equations using Boussinesq and hydrostatic approximations. The conservation laws for heat, salt, and momentum are written in the orthogonal curvilinear coordinates and physical z-vertical coordinate system. The tracer advection is based on the multidimensional extension of QUICKEST scheme [42,43]. Some physical processes, which cannot be adequately resolved by the numerical model, are described by parameterizations, such as parameterization of vertical convective and turbulent mixing, formation of slope flows, or cascading [44].

The ocean model is coupled with the sea ice model CICE v3 [45]. The ice model simulates the rheology and multi-category sea ice thermodynamics [46] and advection on the basis of a semi-Lagrangian scheme [47].

Numerical simulations were performed for the modeling domain covering the Arctic Ocean bounded by the Bering Strait, and the Atlantic Ocean north from 20 °S. The three-polar numerical grid has a resolution of 0.5° in the Atlantic Ocean and from 10 to 25 km in the Arctic, with about 15 km in the Arctic shelf seas. The vertical grid consists of 38 levels. The minimum shelf depth is 12.5 m.

NCEP/NCAR atmospheric reanalysis data [48] were used to set forcing at the ocean and sea ice surfaces. The initial fields of temperature, salinity, current velocity, and sea ice distribution for 2016 were taken from the results of our previous calculations using the SibCIOM model [49], carried out since 1948.

Water inflow at open boundaries has a prescribed transport, temperature, and salinity. The incoming Bering Strait water has characteristics recommended by climatology data from [50]. The river discharge corresponds to the [51] database. Monthly mean discharge data for the largest Arctic rivers (Lena, Yenisey, Ob, Pur, Kolyma, Yana, Indigirka, Olenek, Northern Dvina, Pechora, Mackenzie) were taken from the ArcticGRO (Arctic Great Rivers Observatory) Discharge Dataset [52] for the period from 2016 to 2020. Monthly average temperatures of Eurasian rivers were obtained from Arctic River Discharge and Temperature (ARDAT) dataset [53].

The SibCIOM model was tested in coordinated experiments of the international project FAMOS (Forum for Arctic Modeling and Observational Synthesis [54]) and in comparisons with observational data [55–57]. The model results [41,58,59] showed that SibCIOM is able to simulate the interannual and seasonal variability of the water and sea ice in the Arctic Ocean and the Arctic shelves. For this study, we used ocean and sea ice dates simulated by the SibCIOM for the five year period of 2016–2020. Analysis of these results and comparison with the observations have been presented in our recent studies [59–61].

2.2. Method of Simulation of Microplastic Transport

The distribution of microplastics in the marine environment was modeled using the Lagrangian particle tracking model. The basic displacement of the passive tracer in the model was determined to be $dr = Udt$, where $dr(dx, dy, dz, t)$ is the displacement, $U = (u_{ocn}, v_{ocn}, w)$ defines the particle velocity when the tracer was in the water, and $U = (u_{ice}, v_{ice}, 0)$ if movement of particles freezing into ice was considered. The values of the horizontal velocity components u_{ocn}, v_{ocn} were provided by the large-scale ocean model. The vertical velocity was calculated as $w = w_{ocn} + w_s$, where w_{ocn} is ocean velocity in the vertical direction, and w_s is sinking or rising velocity of the MP particles determined based on their properties. Marine microplastics show wide range of densities, sizes, and shapes that determine their buoyancy. In this study, the vertical velocity of the particles was calculated according to [62]

$$w_s(x, y, z, t) = \frac{v}{2R} d^3 \left(38.1 + 0.93d^{12/7} \right)^{-7/8}, \quad (1)$$

where

$$d = 2R \left(\frac{g}{v^2} \frac{\rho_p - \rho_{ocn}}{\rho_{ocn}} \right)^{1/3}. \quad (2)$$

Here, ρ_{ocn} is the three-dimensional seawater density from SibCIOM model results, g is the gravity, ρ_p is the plastic density, R is the particle radius, and v is kinematic viscosity.

2.2.1. Ice Freezing and Melting

Freezing and melting of sea ice are among the most fundamental processes that determine the state of the water masses in the Arctic Ocean. Plastic particles located in the ocean surface layer can be frozen into the ice and move via the ice drift. With the summer onset and ice melting, MPs release into the water.

To determine the freezing rate of microplastic particles, we relied on the works [35,36]. These papers describe laboratory experiments for studying the freezing of microplastic beads into ice. The study [35] considered the process of entrainment of microplastic beads into sea ice based on laboratory experiments with the freezing of Antarctic water. Analysis of the MP distribution in the ice and water after 15 days of the experiment showed that the percentage of microplastic entrainment into the ice varied from 10 to 50% and correlated with the salinity of the water and sea ice. A similar study carried out in [36] showed a greater degree of microplastic freezing: the proportion of microplastics in the ice was about 77% after 24 h. The results obtained in these studies did not provide us with the certainty to allow for parameterization of this process in the ocean and sea ice model. However, it was clear from both studies that microplastics are actively frozen into ice in a relatively short period of time.

We assumed that daily probability of plastic inclusion into ice is estimated to be 10%, provided that the ice freezes and the local ice area exceeds 50% concentration. The possibility of MP release into water during ice melt for every grid point was estimated as $P = \frac{\Delta V_i}{V_i}$, where $V_i(x, y, t)$ is ice volume and $\Delta V_i(x, y, t)$ is the local ice volume change due to melting over time Δt . The change due to melting is estimated based on the melting rate of the ice in each model grid cell. This does not consider changes in ice volume due to transport.

2.2.2. Biofouling

Data on the dynamics and timescales of biofouling of plastic are limited. Biofouling sufficient to sink buoyant microplastics has been described theoretically in [63], where some approximate estimates of the basic spatial and temporal scales describing the particle behavior of different densities and shapes in the Baltic Sea were obtained.

Considering biofouling, which leads to an increase in average particle density and sinking rate, the authors found that for spherical particles, with a constant fouling rate proportional to surface area, the time to fouling to water density is directly proportional to the radius of the sphere. Based on the findings of [63], the change in particle density with biofouling was calculated using the formula

$$\rho_p = \rho_0 \frac{R_0^3}{(R_0^3 + BT)^3} + \rho_b \left[1 - \frac{R_0^3}{(R_0^3 + BT)^3} \right], \quad (3)$$

where R_0 is the initial radius of the particle, ρ_0 is the density of the polymer, ρ_b equals 1.38 g/cm^3 in the experiments (as proposed in [64]), and $BT = BT_0 + BR \cdot \Delta t$ is the thickness of biofouling, the change in which over time is determined by the biofouling rate BR and the initial biofilm thickness BT_0 .

It was also assumed that the biofouling rate depends on the time of year, being maximal in the spring and tending to zero with the onset of winter. The schematic drawings in the work [65] depict a temporal development of ice algae and phytoplankton blooms. By analyzing these drawings, we created a functional relationship to determine the time dependence of the biofouling rate for microplastic particles as

$$BR = BR_{\max} \cdot f, \quad (4)$$

where BR_{\max} is maximum value of biofouling rate, and f equals f_{ice} or f_{ocn} , depending on particle location, and describes seasonal variability of biofouling as follows:

$$f_{ice} = \frac{1}{3} \cdot \begin{cases} e^{(t-t_{ice})/10}, & t \leq t_{ice} \\ e^{-[(t-t_{ice})/10]^2}, & t > t_{ice} \end{cases}, \quad (5)$$

$$f_{ocn} = \begin{cases} e^{-[(t-t_{ocn})/20]^2}, & t \leq t_{ocn} \\ e^{-(t-t_{ocn})/20}, & t > t_{ocn} \end{cases}. \quad (6)$$

Here, t denotes time in days. Our study used $t_{ice} = 140$ and $t_{ocn} = 165$ days.

3. Experimental Design

The transport of MP particles was simulated during the 2016–2020 period using data on the state of the Arctic Ocean obtained from 3D numerical modeling, namely the daily averaged ocean arrays of velocity, temperature, salinity, and sea ice arrays of thickness, concentration, drift velocity, and ice melting rate.

We simulated the transfer of microplastics entering the Kara Sea shelf area with the waters of the Yenisey and Ob rivers. To determine the source of microplastics, we relied on the model study [26] based on analyses of population density and the quality of plastic waste disposal systems in the catchment area. In this paper, the average annual volume of pollution discharge was evaluated as 795.55 t/year for the Ob and 117.85 t/year for the Yenisey [26]. To model the Lagrangian transfer of MPs, we assumed that each particle is associated with a volume of microplastics equal to 5 t. Thus, 182 particles enter the region each year, which is sufficient to illustrate the main features of the particle distribution in the region. The particles were released simultaneously during the simulation period. The estimate of daily particle output to the seawater was based on the daily distribution of the annual river load of microplastics calculated in accordance with the monthly river discharge [51].

A series of sensitivity experiments based on the same hydrological characteristics were carried out. The following parameters were varied: plastic type, particle size, probability of freezing in sea ice, and biofouling rate. Of the seven most common types of microplastics [37], three types were considered, namely high-density polyethylene (HDPE, density 955 kg/m^3), polypropylene (PP, density 1010 kg/m^3), and polystyrene (PS, density 1040 kg/m^3). The first two types of microplastics (HDPE and PP) have a density lower than that of seawater and are classified as buoyant plastics. Polystyrene (PS) has a density greater than water density, so it is considered negatively buoyant. Microplastic particles were assumed to be of two sizes, 5 and 0.5 mm. Observations show that all types of MPs were found in the Arctic ice and waters [66]. Polyethylene is one of the most frequently found microplastics in the Arctic ice (21% , size $20 \text{ }\mu\text{m}$ – 2 mm [13]; 57%, size 0.1 – 5 mm [66]).

First, the control experiment included all types of MPs (HDPE, PP, and PS). In the experiment, riverine microplastics were carried by the ocean currents, so the particles could be incorporated into sea ice during ice freezing, transported via ice drift, and released back into the water during ice melt. Biofouling was not considered in the control experiment.

The second series of experiments was carried out to study whether biofouling influences the transport of buoyant microplastics (HDPE, PP) and results in their removal from surface waters. To investigate the effect of biofouling on MPs, we used three values of the maximum biofouling rate to calculate its seasonal distributions, namely 10^{-4} , 10^{-3} , and 10^{-2} mm/day . These values were chosen to reproduce the time period when biofilm on plastic becomes visible [67]. The third sensitivity simulation focused on MP size. At the same time, all plastic choices and all biofouling rate options were considered for each particle size. Figure 3 shows an illustration of the sensitivity experiments.

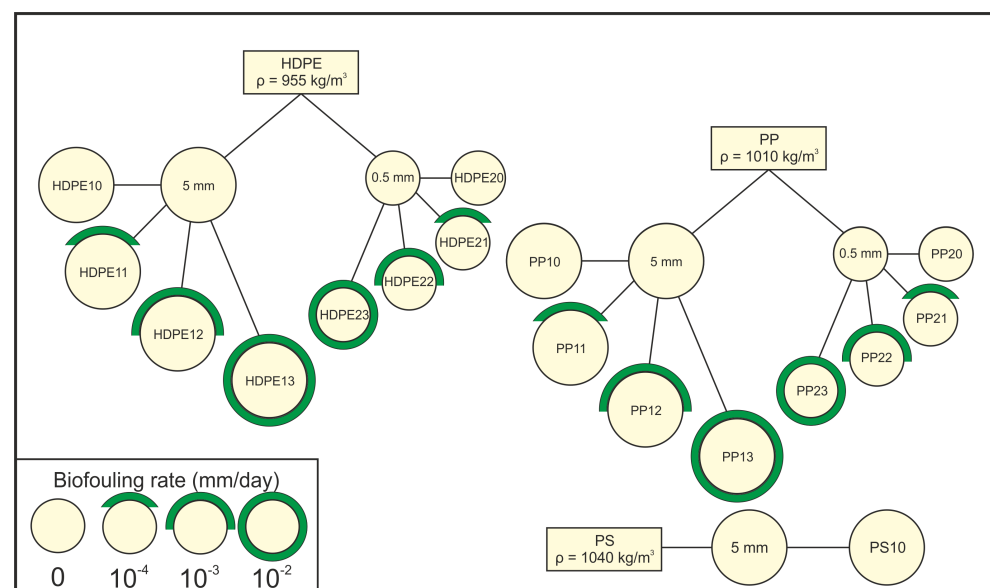


Figure 3. Illustration scheme of experiments on sensitivity to MP type (plastic density), particle size, biofouling rate. The experiment name is given by the type of plastic (HDPE, PP, or PS) followed by two digits, the first defining the particle size: “1” for 5 mm and “2” for 0.5 mm; the second digit defines maximum biofouling rate BR_{\max} , namely “0”—no biofouling, “1” for 10^{-4} mm/day , “2” for 10^{-3} mm/day , and “3” for 10^{-2} mm/day .

At the end of our study, several experiments investigated the effect of the microplastics’ incorporation into sea ice. A few values for specifying the probability of particle freezing were tested, namely $P = 0, 0.01, 0.1,$ and 0.9 . The sensitivity study was conducted for the lightest HDPE microplastic with a particle size of 5 mm. A biofouling rates of 10^{-3} mm/day and 10^{-4} mm/day were used that allowed a number of particles to hold in the surface layer.

4. Results

4.1. Control Experiment: Biofouling Excluded

The main drivers of microplastic transport in the ocean are water circulation and ice drift. Sea ice is the most dynamic part of the ice–ocean system of the Arctic Ocean. Under the action of wind, its drift can change quite rapidly, even to the opposite direction. Figure 4 presents the two most characteristic types among the numerous variants, simulated by the numerical model: anticyclonic and cyclonic. In both cases, despite the opposite direction of circulation, there is a flow carrying sea ice from the Arctic Ocean to the Greenland Sea through the Fram Strait.

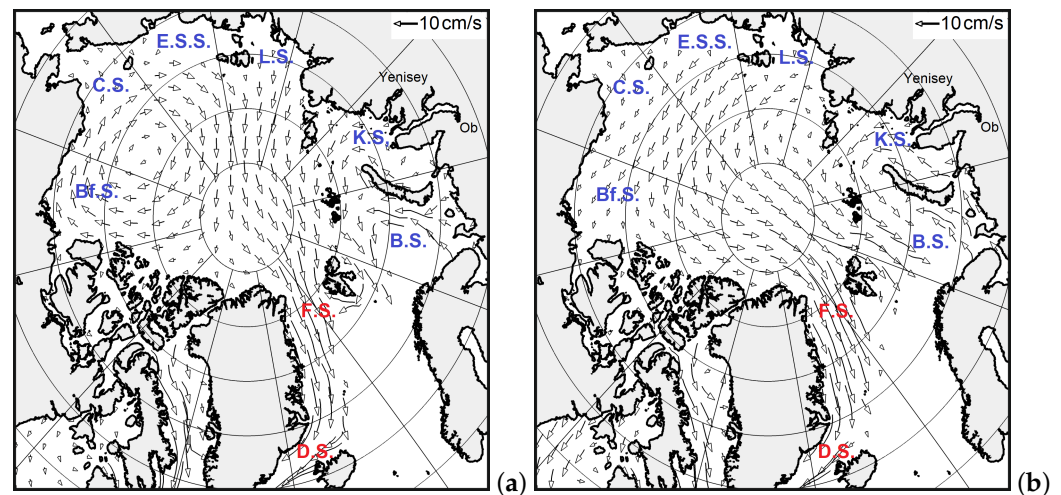


Figure 4. Simulated in SibCIOM two modes of ice drift, (a) anticyclonic; (b) cyclonic. Here, B.S.—Barents Sea, K.S.—Kara Sea, L.S.—Laptev Sea, E.S.S.—East Siberian Sea, C.S.—Chukchi Sea, Bf.S.—Beaufort Sea, F.S.—Fram Strait, D.S.—Denmark Strait.

The circulation of the surface water layer of the Arctic Ocean and its shelf seas is not a repetition of the ice drift pattern, as it is formed on the basis of a complex system of interactions with ice, the atmosphere, incoming fresh water flows, and waters of the adjacent sea areas. In the numerical model, the propagation of the Ob and Yenisey tracers in the shelf water occurs mainly along two trajectories: the eastern one characterizes the jet along the coast of Eurasia with an exit through the Vilkitsky Strait into the deepwater part of Laptev Sea, and the second trajectory passes along the central and western part of the sea in the direction of the strait between the islands of Franz Josef Land and Severnaya Zemlya. The intensity of the two branches is different in different years and may change during the year. The surface circulation in Figure 5a demonstrates the velocity field averaged over the simulated period of 2016–2020; therefore, both branches are visible simultaneously in the figure. As a rule, in the conditions of the established ice cover, from November to July, the main distribution of tracers occurs along the coast of Eurasia in the direction of the Vilkitsky Strait. When the sea is free from ice, the dynamic state of the atmosphere is the determining factor in establishing the surface circulation. A common feature of the surface circulation and ice drift is the export of surface water from the deep Arctic basin to the Greenland Sea.

Figure 5b represents the water circulation in the Eurasian basin in the 200–600 m layer, which is characterized by the propagation of Atlantic waters along the continental slope in a cyclonic direction. The same figure shows the second branch of Atlantic waters in the bottom layer of the Barents Sea.

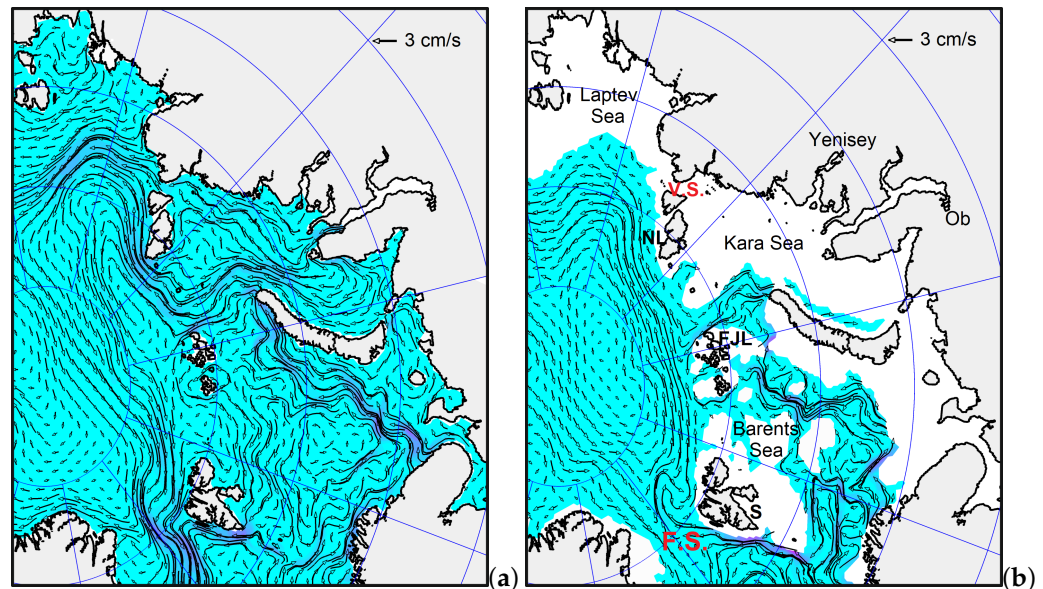


Figure 5. Large-scale velocity fields averaged over the 2016–2020 period (SibCIOM results): (a) mean in the surface layer 0–10 m; (b) mean in the layer 200–600 m.

The analysis of the modeling results of the five-year continuous microplastic riverine inflow showed that light plastic particles, regardless of their sizes (experiments HDPE10, HDPE20, PP10, PP20), spread throughout the Arctic Ocean in a similar way, predominantly staying in the surface layer (Figures 6a and S1a–d). Repeatedly moving from the upper layer of water to ice and back, they move both in the Kara Sea and beyond. Depending on the direction of surface water circulation, in certain periods, flows are formed through different straits, which connect the Kara Sea with the surrounding waters. Once off the shelf, the particles are included in the large-scale circulation system of the Arctic Ocean. The general direction of ice drift and surface circulation force them through the Fram Strait and further through the Denmark Strait into the Atlantic Ocean, including in a frozen-to-ice state. The appearance of particles in the Barents Sea is caused by ice drift, as will be shown in the subsequent section analyzing the role of sea ice.

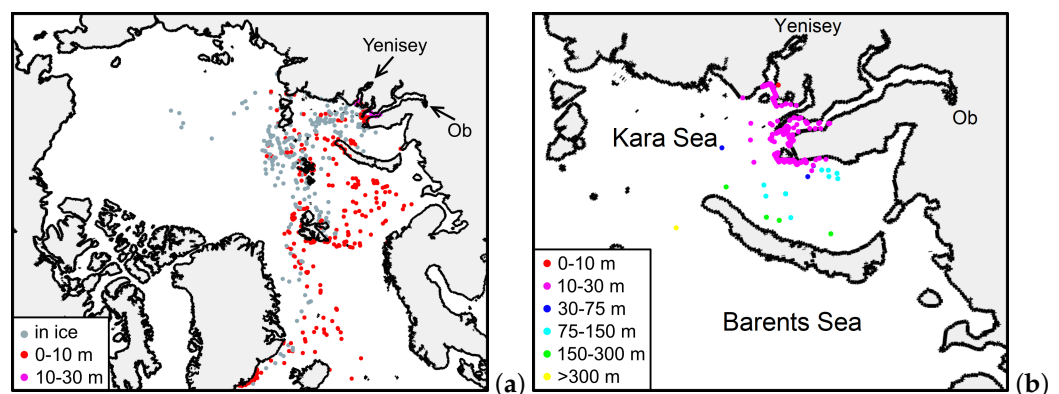


Figure 6. Simulated particle distribution after 5 years of continuous riverine MP influx. Biofouling is excluded from consideration. (a) Results for PP, particle size 0.5 mm; (b) PS, particle size 5 mm.

Small differences can be noticed near the estuaries, where waters are characterized by low salinity and correspondingly low density compared with waters in more distant regions. In contrast to HDPE, which are floating, a small portion of PP particles settle near the river mouth because they have a density greater than the surrounding waters (Figures 6a and S1).

Heavy plastic PS particles, being carried out with river waters, settle in the immediate vicinity of the river mouth and are transported via a system of bottom currents over a short distance across the Kara Sea. Moreover, not a single PS particle was captured by ice over the five years of calculation. Figure 6b shows the distribution for a PS particle size of 5 mm. From the Formula (1) that determines the rate of particle immersion, it follows that smaller particles are deposited faster. In further experiments, PS is excluded from consideration due to its high density, which leads to the rapid immersion of particles even without biofouling.

4.2. Sensitivity Tests to Biofouling Rate and Particle Size

The sensitivity to biofouling was tested in experiments for two types of microplastics (PP and HDPE) considering particle sizes of 5 and 0.5 mm. The maximum value of the biofouling rate varied by 10^{-4} , 10^{-3} , and 10^{-2} mm/day. Due to biofouling, the rate of particle immersion changes along with the corresponding pattern of particle distribution in the sea. For demonstration purposes, the most representative distributions of microplastic particles at the end of the five-year modeling period were selected.

Considering the highest biofouling rate for our experiments, $BR_{max} = 10^{-2}$ mm/day, the simulation shows that the main pollution is concentrated on the seafloor of the Kara Sea. The MP particles of all sizes and all types are deposited (Figure 7).

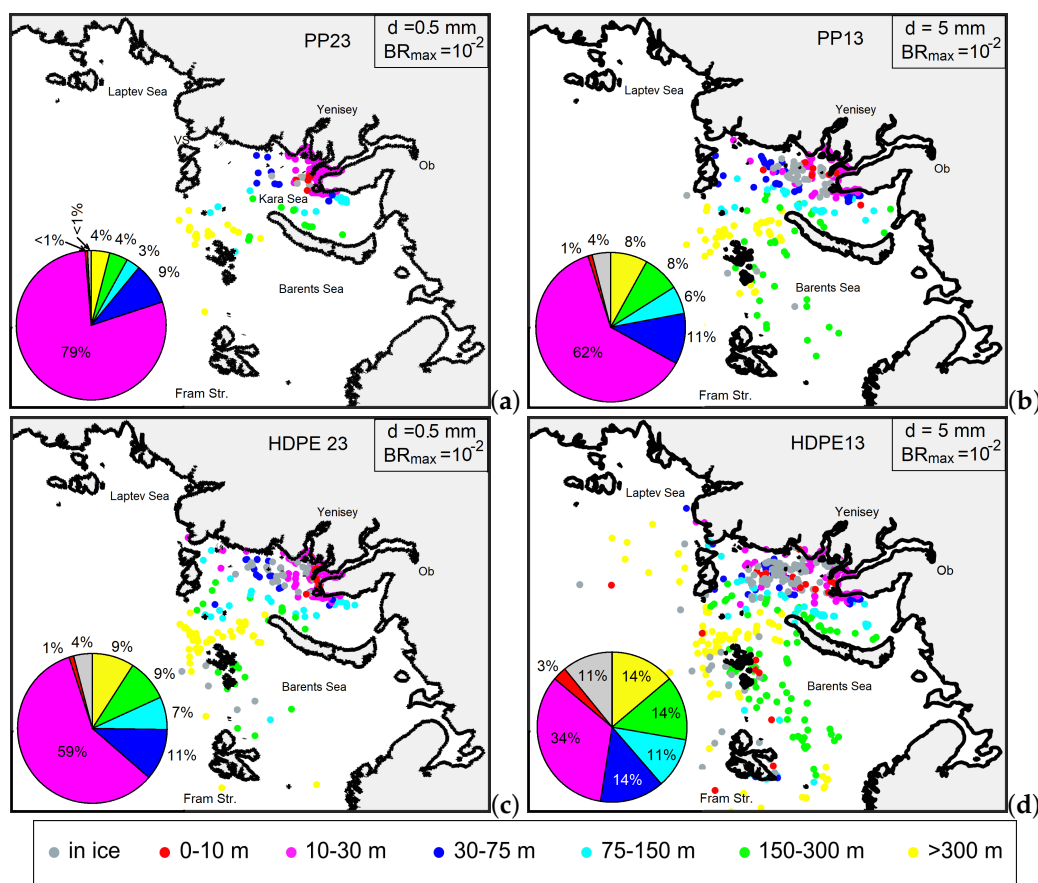


Figure 7. Simulated microplastic particle distribution after 5 years of continuous riverine influx. Biofouling rate: $BR_{max} = 10^{-2}$ mm/day. Particle size: 5 and 0.5 mm. Results of the experiments: (a)—PP23; (b)—PP13; (c)—HDPE23; (d)—HDPE13. Particle color is determined by its immersion depth, shown in the panel below. The circle diagram shows the percentage of the particles in each layer.

PP particles, at a size of 0.5 mm (Figure 7a), are concentrated mainly in the area of river mouths. As the particle size increases or lighter HDPE is considered, the pollution

becomes more widely distributed over the Kara Sea, with a small number of particles being deposited on the shelf of the Barents Sea (Figure 7b,c). The distribution for 5 mm HDPE not only shows shelf pollution but also includes some particles that have reached the deep-water part of the basin (Figure 7d).

Reducing the biofouling rate to 10^{-3} mm/day allows floating particles to be retained in the surface layer of water and spread via surface currents. A significant portion of 5 mm PP particles settle on the shelf (PP12, Figure 8a), but their distribution area is wider than in the PP13 experiment (Figure 7b).

Lighter 5 mm HDPE particles not only fill the shelf area, but also extend into the deep-water part of the Arctic Basin (HDPE12, Figure 8b). Moving to the south, they pass through the Fram Strait, deepening into the Greenland Sea. In contrast to HDPE, the inclusion of PP particles in the ice cover is mainly observed in the central part of the Kara Sea. Intensive model transport into the Barents Sea during the calculation period leads to pollution of the region, which, unlike in the situation presented in (Figure 6a), is concentrated in the bottom layer of the sea.

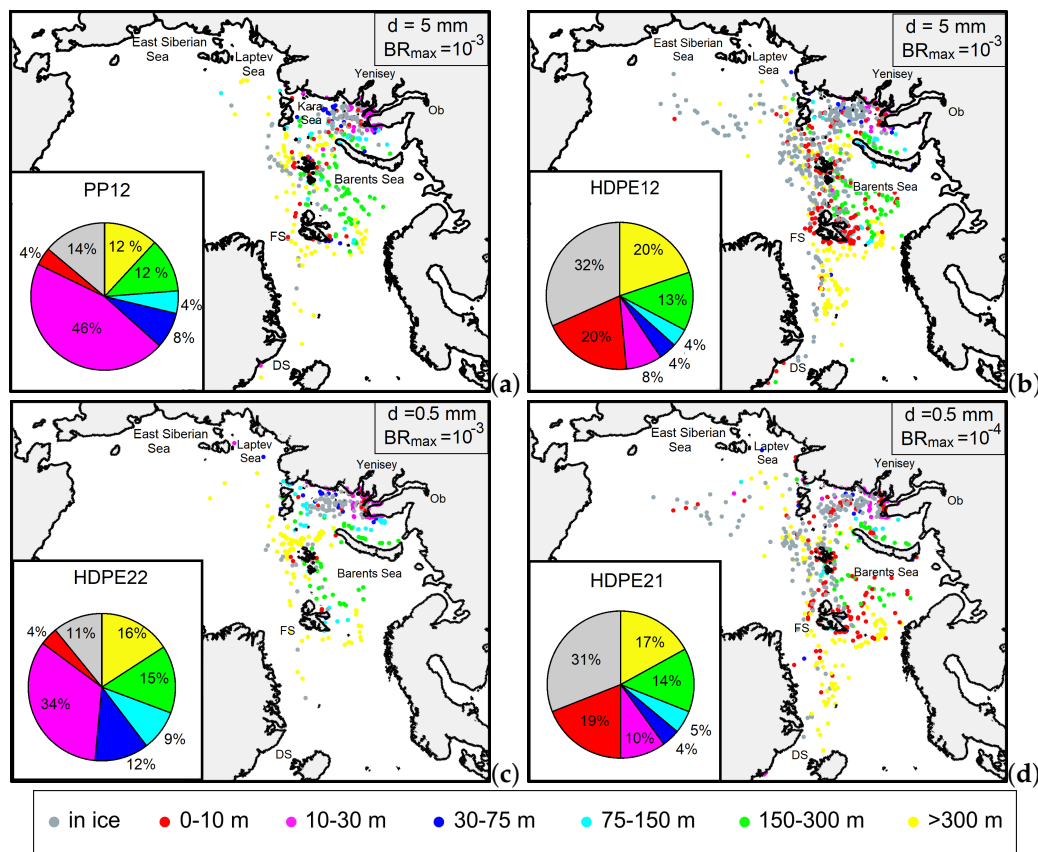


Figure 8. Simulated microplastic particle distribution after 5 years of continuous riverine influx. Different particle sizes and biofouling rates. Results of the experiments: (a)—PP12; (b)—HDPE12; (c)—HDPE22; (d)—HDPE21. Particle color is determined by its immersion depth, shown in the panel below. Type of MP differs in (a) and (b); (b) and (c) differ in particle sizes; (b) and (d) differ in particle sizes and biofouling rates; (c) and (d) differ in biofouling rates. The circle diagram shows the percentage of the particles in each layer. Here, FS—Fram Strait, DS—Denmark Strait.

The trajectories of several 5 mm HDPE particles are shown in Figure 9. The inset illustrates the change in immersion depth of the corresponding particle over time. The particle marked with the red line traveled the farthest distance and reached the Denmark Strait. It entered the shelf in winter and was frozen into the ice. Moving with the ice, it exited the Kara Sea through the Vilkitsky Strait and was included in the Transpolar Drift. The particle was embedded in the ice most of the way. The other particle whose trajectory is marked

with a brown line traveled almost the same path; it was also mostly in the ice. But, after passing through the Fram Strait, it shifted eastward and ended up in the water due to melting ice, where it quickly sank to the bottom under the effect of biofouling. Particles entering the shelf in the summer, under the influence of biofouling, end up in the bottom layer of the shallowest part of the shelf in the first year (magenta line). The behavior of particles that managed to escape beyond the estuary region is more complex. Their gradual submergence can be oscillating (green line), since the submergence rate is determined not only by the properties of the particle but also by the density of the water in which it is currently located.

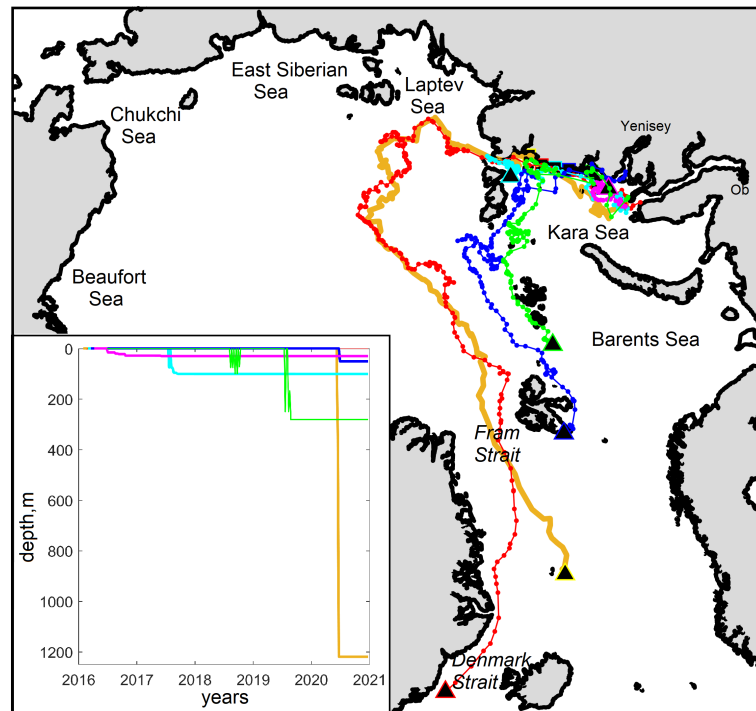


Figure 9. Simulated 6 most different trajectories of microplastic particles shown in different colors. The triangle shows where the particle was in December 2020. HDPE12 experiment (5 mm particles, biofouling rate $BR_{max} = 10^{-3}$ mm/day). The inset illustrates the change in immersion depth of the corresponding particle over time.

The reduction in particle size leads to an increase in sedimentation under the same biofouling rate. Figure 8c for the HDPE22 experiment shows that a significant portion of the 0.5 mm HDPE particles ended up in the bottom layer after a five-year period. The approach used (Formula (3)) suggests that a reduction in particle size will result in an increase in MP particle density regardless of biofouling intensity.

Figure 10a shows the dependence of HDPE particle density on size at a constant biofilm thickness. The consideration of seasonal biofouling (Formulas (4) and (6)) enhances the differences between the density changes for particles of different sizes. Figure 10b shows a more intensive density increase for smaller particles within one year for the same maximum value of the biofouling rate. It is also worth noting that at $BR_{max} = 10^{-4}$ mm/day, the density of HDPE particles does not reach critical values exceeding the density of the surrounding seawater within one year. The particle can thus remain in the surface layer of the seawater. More intensive biofouling (Figure 10c) results in the particle density exceeding the density of the seawater by the autumn season, contributing to its submergence.

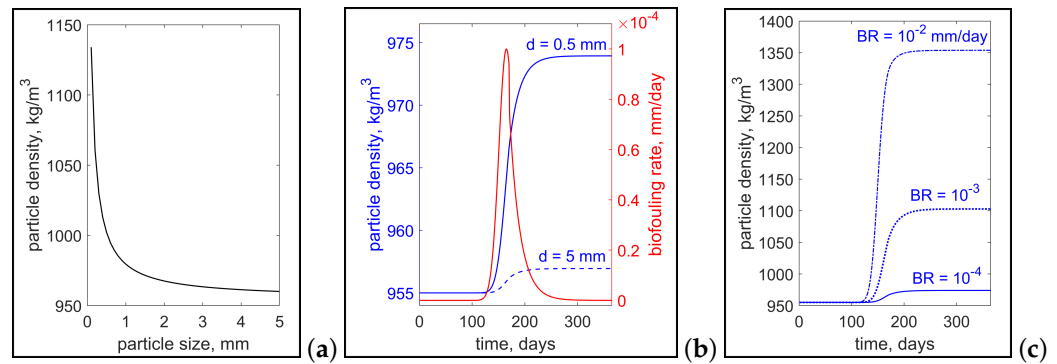


Figure 10. Density change of MP particles via the Formula (3). (a) Dependence of particle density on particle size at constant biofilm thickness $BT = 0.1$ mm; (b) change in density of 5 mm (blue dashed line) and 0.5 mm (blue solid line) particles during a year at the same biofouling rate (red line) with the maximum value of $BR_{max} = 10^{-4}$ mm/day; (c) change in density of 0.5 mm particles during a year at biofouling rates $BR_{max} = 10^{-4}$ mm/day (solid line), 10^{-3} mm/day (dotted line), and 10^{-2} mm/day (dash-dotted line). HDPE particles were considered in all cases.

Time series in the Figure 11 demonstrate the change in the vertical position of HDPE particles during the simulated period depending on particle size at the same biofouling rate. The plots reflect the number of particles in a certain layer on the shelf and in the deep-water region. Figure 11a shows that 5 mm particles can stay in the surface layer for quite a long time. The opposite behavior of the red and black lines, corresponding to the number of particles in the surface ocean and ice layers, shows that particles move from the surface to the ice and back into the surface layer. Figure 11a shows that the process of 5 mm particle deposition in the shelf region is rather slow. The appearance of 5 mm particles in the deep-water part of the Arctic Ocean started after one year (Figure 11b). From the plot shown, it can be concluded that the major part of the pollution in the deep water is due to the transport of particles frozen in the sea ice. Further melting of the ice and biofouling of the particles leads to the sinking of particles into the deep layers.

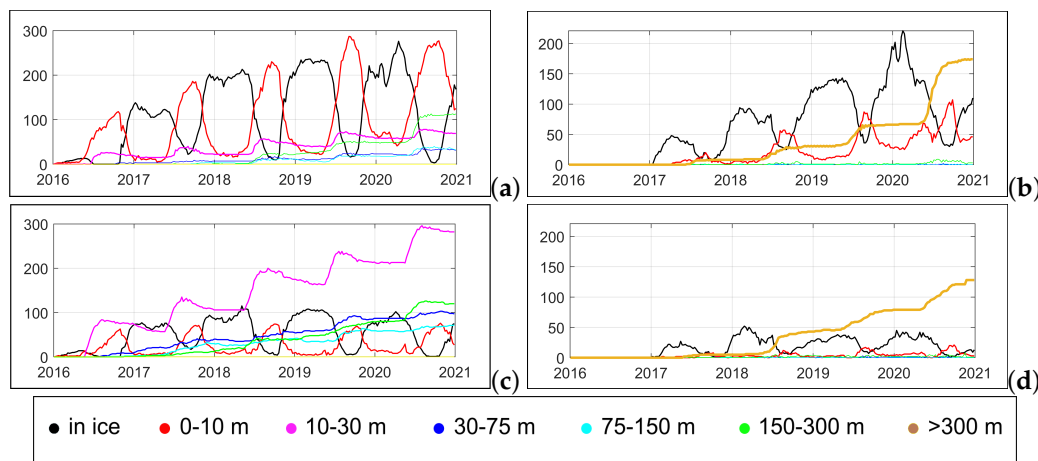


Figure 11. Time series of HDPE particle number in different water layers: (a,b)—particle size is 5 mm; (c,d)—particle size is 0.5 mm; left panels show the number of particles in region where the sea depth is shallower than 300 m; right panels—the same for deep-water regions.

The behavior of the plots corresponding to 0.5 mm particles is significantly different from the plots for 5 mm particles. Figure 11c for the shelf region also shows the opposite behavior of the black and red lines, but the number of particles in the surface layer is much smaller than that in Figure 11a. At the same time, there is an intense accumulation of microplastic particles in the bottom layer of the shelf, especially near the river mouth (purple line). For a given biofouling rate, the sinking rate of smaller particles is greater.

Particles are also transported into the deep basin with the ice cover (Figure 11d). Their amount is much smaller and there is no accumulation effect which can be seen for the 5 mm particles in Figure 11b. Here, as well as in the shelf region, a more intensive submergence of particles during ice melting can be observed.

A further decrease in the biofouling rate to 10^{-4} mm/day allowed 0.5 mm HDPE particles to remain in the surface layer and in the sea ice for a long time before the density of particles within the biofilm reached the ambient density. In the HDPE21 experiment (Figure 8d), the spatial distribution of particles, including the depth of their immersion, was found to be close to the distribution of particles in the HDPE12 experiment (Figure 8b), which used a 5 mm particle size and 10^{-3} mm/day biofouling rate. It should be noted that, for 5 mm particles, using a biofouling rate of 10^{-4} mm/day (HDPE11, Figure S2a) did not produce considerable differences in the resulting particle distribution compared with the HDPE10 calculation without biofouling (Figure S1a).

The spatial distributions of the MP particles for the remaining experiments are presented in the Supplementary Material. Figure 12 shows the distribution of MP particles by the vertical layers at the end of the five-year simulation period for all experiments as a percentage of the total number of particles. Figure 12a demonstrates the same results obtained in the HDPE12 and HDPE21 experiments as well as in the HDPE13 and HDPE22 experiments. In contrast to the HDPE, the distribution of PP results did not exhibit the same correlation (Figure 12b). With the exception of experiment PP11, which had the slowest biofouling rate, all other experiments showed high sedimentation rates in the shallowest part of the shelf. It is worth noting that reducing the particle size of PP microplastics leads to more intense particle sinking than increasing the rate of biofouling. If PP microplastic particles are mechanically broken down, they will settle to the bottom even with a minimal level of biofouling.

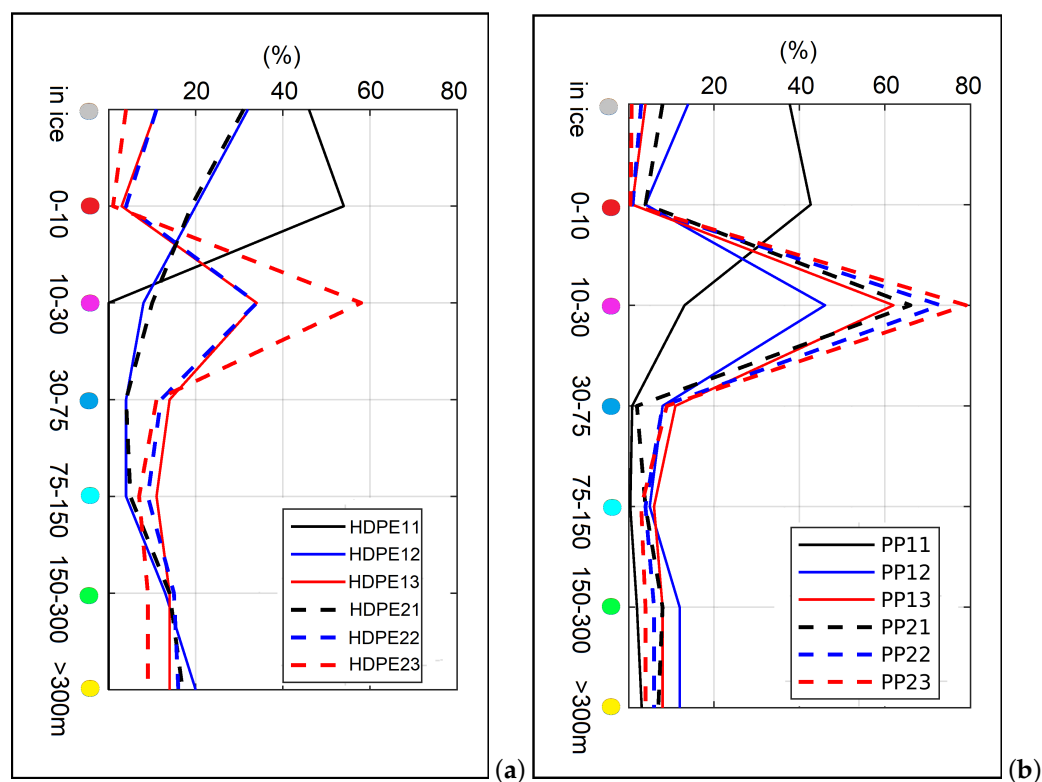


Figure 12. Distribution of MP particles by the vertical layers at end of the 5-year simulation period as a percentage of the total number of particles. (a)—HDPE experiments; (b)—PP experiments. The solid lines correspond to particles of size 5 mm; the dotted lines corresponds to 0.5 mm.

4.3. Sensitivity of MP Transfer to Freezing into Sea Ice

A series of numerical experiments were conducted to investigate the sensitivity of the microplastic incorporation into sea ice. Since the parameterization of this process is currently undefined, several values for specifying the probability of particle freezing were tested, namely $P = 0$; 0.01; 0.1; and 0.9. Sensitivity experiments were conducted for the lightest HDPE microplastic with a particle size of 5 mm and a biofouling rate of 10^{-3} mm/day, allowing the particles to hold in the surface layer. The simulation results show that by varying the probability value from 0.1 to 0.9, the spatial distribution after a five-year result has a basically similar pattern (Figure 8b for $P = 0.1$ and Figure S4d for $P = 0.9$). Significant differences in the particle distribution appear when the probability approaches zero. The distributions obtained for $P = 0$ and $P = 0.01$ (Figure 13a,b) are similar to each other and significantly different from the same pattern for $P = 0.1$ (Figure 8b). In the absence of particle involvement in the ice, their transport is only due to water circulation and additional submergence caused by biofouling. Most of the particles settle on the Kara Shelf. The particles that leave the sea, under the influence of biofouling, reach the layer of Atlantic waters spreading in the cyclonic direction (Figure 5b). Transported in the Atlantic layer, they settle on the continental slope of the Eurasian basin (yellow dots in Figure 13a,b). These two experiments ($P = 0$ and $P = 0.01$) show that even the minimal incorporation of particles into the ice favors their wider spreading across the Kara Sea.

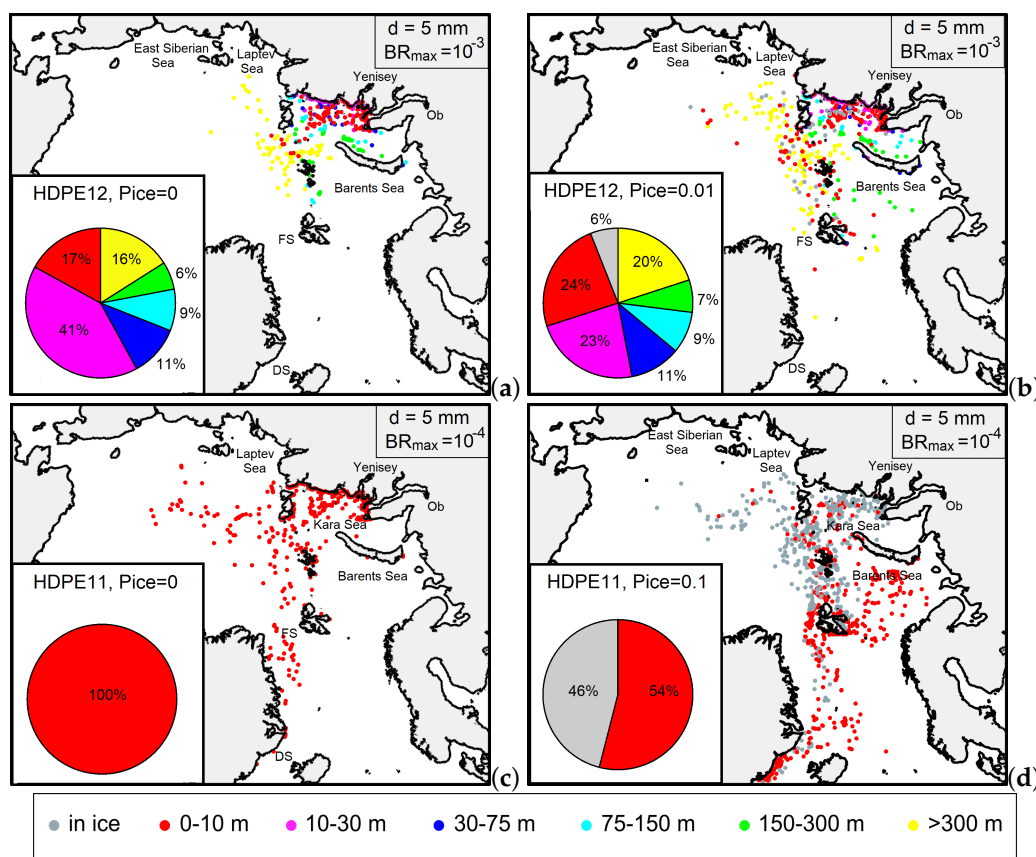


Figure 13. Sensitivity of HDPE MP distribution to the probability of freezing into sea ice: (a) $P = 0$, biofouling rate of 10^{-3} mm/day; (b) $P = 0.01$, biofouling rate of 10^{-3} mm/day; (c) $P = 0$, biofouling rate of 10^{-4} mm/day; (d) $P = 0.1$, biofouling rate of 10^{-4} mm/day. The circle diagram shows the percentage of the particles in each layer.

The importance of considering microplastic particles freezing into ice is most apparent when comparing the results of two simulations for the minimum biofouling rate, 10^{-4} mm/day, which does not lead to the particle sinking into the deep layers during the five-year period. In the absence of freezing (Figure 13c), particles in the surface layer

are concentrated along the Kara Sea coastline and carried to the central ocean and to the Greenland Sea through the Fram Strait. At $P = 0.1$, the model results show a more intensive export of particles outside the Kara Sea. The export through the Fram Strait and the Denmark Strait is clearly expressed (Figure 13d). In addition, the model shows that the transport of particles with ice drift leads to the export of pollution to the Barents Sea through the strait east of Spitsbergen. These particles are then transported across the Barents Sea by the current system. The differences noted in the pollution of the Barents Sea due to the transfer of microplastics by sea ice also apply to the experiments considered above with a biofouling rate of 10^{-3} mm/day (Figure 13b).

5. Discussion

In this study, we tried to determine how sensitive the distribution of microplastics in the Arctic waters is to some physical and biological processes. Our research shows that the process of introducing microplastics into the ice has a significant impact on particle trajectories. The circulation of the upper ocean may differ from that of ice drift. Ice drift is the most dynamic part of the ice–ocean system, strongly influenced by wind, but ocean circulation is defined as the result of a complex system of interactions with sea ice, the atmosphere, river inflow, and water masses from adjacent ocean areas. Therefore, the transport of microplastics from the freeze-up to the melt season depends significantly on whether the plastic is in the water or frozen in the ice. Our studies have shown that considering the freezing of particles in sea ice is essential, but the probability of freezing from 10 to 90% per day does not have a significant effect on the final result of microplastic distribution. The greatest difference of the results was obtained when the probability of particle freezing approached zero (1%).

Including the process of microplastics freezing into ice, we obtained an interesting effect of light microplastics spreading into the Barents Sea. Earlier studies indicated that the influx of Atlantic waters is a source of pollution in the Barents Sea [15]. Our research shows that there is also an additional influx of microplastics caused by ice transport from other areas. According to the results of the experiments, the ice entering the Barents Sea east of Spitsbergen melts, and the microplastics it contains enter the water and are transported by the current system or settle on the seafloor due to biofouling. The modeling study [37] also showed that the buoyant microplastics trapped in the sea ice are transported across the Barents Sea and north of Spitsbergen, as well as by the Transpolar Drift through the Fram Strait. The risk of contaminants in the Kara Sea entering the food webs of the Greenland and Barents Seas was reported in the study [68], in which the authors estimated ice drift in the Arctic using satellite imagery and a reconstruction of air pressure for the 1899–1998 period. They showed that a significant proportion of the sea ice in the Arctic Ocean originates in the Kara Sea and melts in the Greenland and Barents Seas. More recently, analysis of large volumes of subsurface water samples from the Barents Sea has revealed high levels of microplastics in the northern part of the sea, close to the ice edge [69].

One of the few studies devoted to the numerical modeling of the fate of MPs in the Arctic Ocean is the work [39]. The authors used Lagrangian particle advection to simulate the long-term transport of buoyant microplastics from northern European rivers into Arctic waters using results from three-dimensional modeling. As can be understood from the text of the work, the processes of particles freezing into ice and biofouling were not considered. To model the vertical movement of buoyant particles, the authors used a random 10 cm vertical displacement of the particles every hour within the upper 20 m of the water column. As a result of the study, microplastic dispersal was shown along the Eurasian continental shelf, over the North Pole, the Nordic Seas, and accumulation zones over the Nansen Basin, the Laptev Sea, and the ocean gyres of the Nordic Seas. In the contrast to this study, we ran experiments over a period of five years. However, our simulations included the processes of particles freezing in ice and biofouling. This led to a different pattern of particle distribution. Nevertheless, we see common features, such as

the spread of microplastics along the continental slope of Eurasia. This process would be more pronounced in our results when modeled over a longer period.

Understanding the processes by which microplastics freeze in sea ice and are transported in its drifting system is crucial for Arctic climate research. The presence of microplastics in sea ice can alter the melting rate by changing the albedo of the ice. However, accounting for these processes requires the coupled modeling of both Arctic hydrology and microplastic spreading. To achieve this, a Eulerian approach to modeling microplastic transport, similar to that used by Mountford and Morales Maqueda [38], would be more appropriate.

Some processes that can affect the transport of particles were not considered in our work. We did not consider the windage of light particles, which, as noted in the work [63], move along the surface of the water, and their drift speed can be up to four times higher in amplitude than the water's current speed and can differ in direction. Intuitively, this makes it possible for light microplastic particles to move faster under the influence of wind even beyond the shelf. It is quite simple to include this process in calculations as an additional particle velocity and it will be accounted for in further studies.

In our work, we considered a simple parameterization of the biofouling process. A more sophisticated and physically based approach modeled the growth of attached algae as being dependent on several processes [70]. These include particle-algae collision, temperature and light dependence, algal respiration, and algal mortality. This approach is likely to have an impact on the temporal extent of floating microplastic particles in surface waters. We also plan to use this approach in a future study.

The work [34], based on laboratory experiments, shows that, similarly to the biofouling of light MPs in surface waters, the aggregation and/or formation of gas bubbles on heavy (usually hydrophobic) plastic particles in the water column or sediments can serve as a mechanism for the vertical movement of MPs. The authors suggest that this mechanism is the most important process facilitating the rise of MPs to the surface and plays a key role in the capture of heavy plastic particles by both fresh water and growing sea ice, since a significant amount (from 17 to 57%) of plastic particles in both fresh and saltwater bodies were frozen into the ice during its formation. To include this process in a large-scale model, a parameterization of the gas bubble formation during biofouling is required. Currently, this issue awaits our further study.

In this study, we relied on the parameterizations developed for spherical MP items. The limitation to a spherical shape as a first approximation can be reasonable due to the fact that small microplastic particles mainly become more circular as a result of mechanical breakdown [71]. However, most of the microplastic samples detected in the Arctic are fibers [13], and riverine floating microplastics consist mainly of polyester fibers [15]. A recent study [72] suggested that the ocean may be a major source of atmospheric microplastic fibers. Thus, the analysis of another form of microplastics and their possible distribution and accumulation in the ocean is of particular interest and requires further attention.

To summarize the results of the study, we have finalized the illustrative scheme of the experiments performed (Figure 3). The main driving force for the simulated vertical displacement of the MP is the difference in density between the particles and seawater. Floating plastics can remain in the surface layer for a long time. Negatively buoyant microplastics (PS) have a higher density than water. Unlike buoyant particles (HDPE and PP), they begin to sink immediately after entering the sea and accumulate on the sea floor.

The light plastic particles of different sizes behave the same unless biofouling is taken into account. The new scheme (Figure 14) provides information on the sensitivity of buoyant microplastic distributions across experiments. Experiments that have similar results are connected by arrows. The vertical level of the experiment circle is important; i.e., the more particles remain in the Kara Sea, the lower the experiment marker is located.

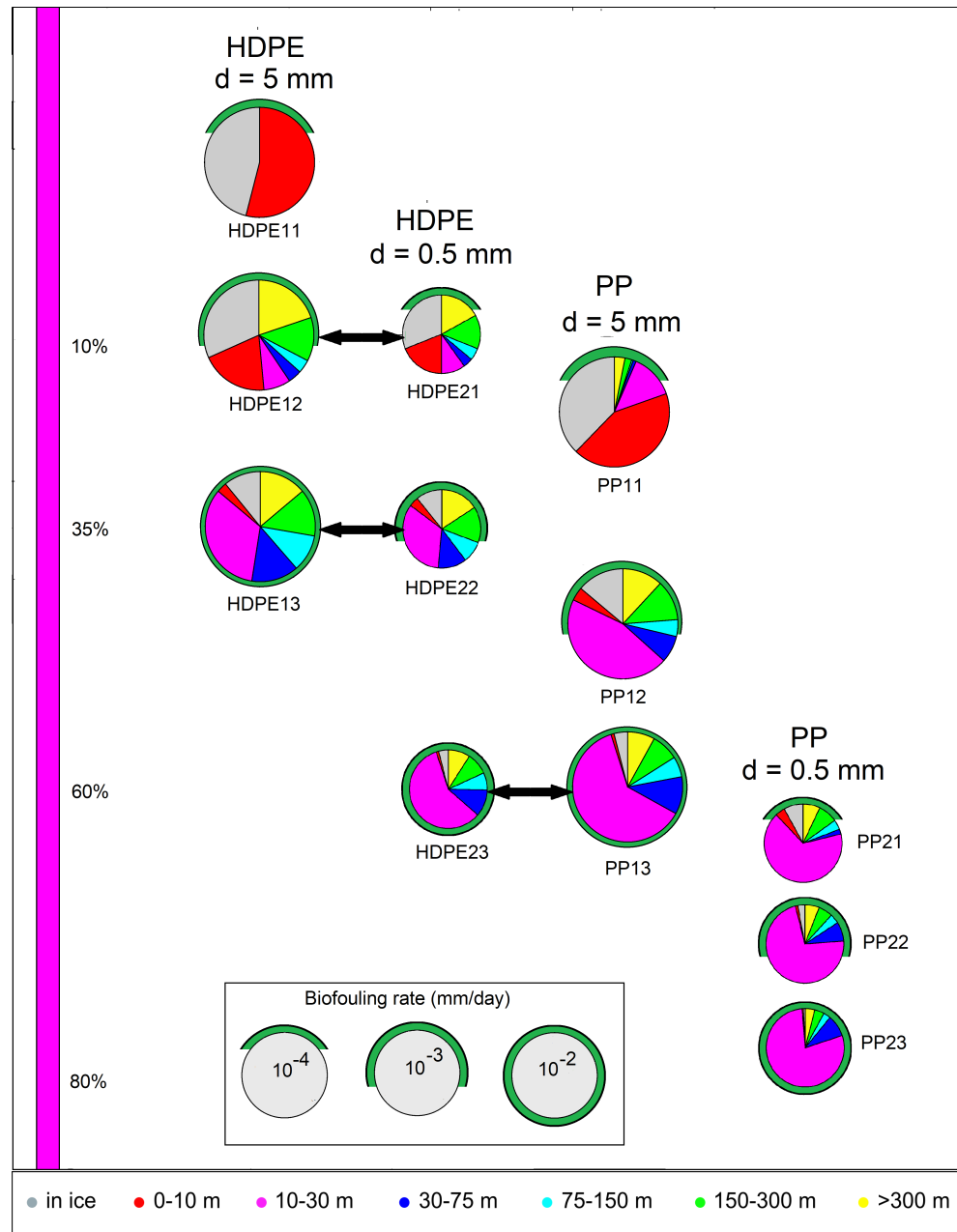


Figure 14. Modified scheme of the sensitivity experiments for the buoyant MPs. Small and large circles denote particle sizes of 0.5 and 5 mm, respectively. The circle diagrams use colors to represent the percentage of MP particles in each vertical layer. Arrows indicate experimental results showing similar microplastic distribution after 5-year calculation. Vertical location of the circles reflects the level of particles sinking in shelf region.

The top position of the HDPE11 circle indicates that MP particles of a large size at a biofouling rate of 10^{-4} mm/day are not deposited in the shelf area, but are carried outside of it. This may account for the prevalence of microplastic particles with sizes around 5 mm in Arctic sea ice [66]. The graph shows that 0.5 mm particles sink faster, so their distribution may be similar to that of 5 mm microplastic particles with a higher biofouling rate or particles of higher density. This means that, during mechanical fragmentation, the MP particles will sink to the bottom more intensively.

We recognize that our approach for the study is an oversimplification of the complex interactions between seawater movement, ice drift, and particle buoyancy as modified by mechanical fragmentation, biofouling, and other factors described in the review [27,33].

We believe that our study focuses attention on fundamental physical processes that need to be studied in order to better identify regions of potential marine microplastic pollution in the future.

6. Conclusions

This study aims to define the most critical physical processes influencing the transport and deposition of riverine microplastics in the Arctic Ocean shelf and deep-water basin. The coupled ice–ocean three-dimensional numerical model SibCIOM and NCEP/NCAR atmospheric reanalysis data were used to obtain daily fields of water and sea ice state and circulation for the period 2016–2020. A three-dimensional Lagrangian particle tracking model used these daily ocean and ice fields to simulate large-scale MP transport. The model included parameterizations of the vertical displacement of floating microplastic particles as a function of the density difference between the particles and the surrounding water, and biofouling (accumulation of microorganisms).

We considered the entire Arctic Ocean domain with riverine microplastic flux from the Yenisey and the Ob into the Kara Sea. Estimates of the amount of plastic entering the ocean with river waters were used from a model based on population density and the quality of plastic waste management systems in the catchment [26]. A series of numerical experiments included three types of microplastics, high-density polyethylene (HDPE, density 955 kg/m^3), polypropylene (PP, density 1010 kg/m^3), and polystyrene (PS, density 1040 kg/m^3), with particle sizes of 5 and 0.5 mm in diameter.

The model simulates the transport of microplastic particles over time and shows that, depending on particle size and density, the particles either float in the water or drift with the ice and sink to the seafloor. The main driver of the modeled long-range transport is ocean and ice circulation, but the vertical displacement of the MP is determined by the difference between the particle and seawater densities. Buoyant plastics can remain in the surface layer for a long time. Negatively buoyant microplastics have a higher density than water. Unlike buoyant particles, they begin to sink immediately after entering the sea and accumulate near the river mouth.

The study emphasizes that the effects of microplastic embedment in sea ice and particle biofouling are fundamental issues that affect the trajectories of floating particles and their settling on the seafloor. Biofouling changes the buoyancy of particles. When the density of a particle with a biofilm exceeds seawater density, it begins to sink. The time a particle remains in the surface layer and the depth to which it sinks depend on the particle size, the rate of biofouling, and the thermohaline structure of the water. Larger particles of 5 mm appear to be more buoyant than the same particles at a size of 0.5 mm. Therefore, the same biofouling rate for 5 and 0.5 mm particles results in different MP distributions.

The modeling results show that low density microplastics repeatedly moving from the upper water layer to the ice and back again are transported both within and out of the shelf. Included in the Transpolar Drift system, they exit through the Fram and Denmark Straits and settle in the deep Greenland Sea depending on the intensity of particle biofouling. The results demonstrate that the transport of light microplastic particles frozen in the ice can lead to the pollution of the Barents Sea from sources located within the Arctic Ocean. Trapped into the ice, microplastics travel faster than in the upper layers of the ocean. Without freezing, less low-density microplastics are transported across the Fram Strait. If we additionally take into account biofouling, which leads to the gradual submergence of floating particles, microplastics remain on the shelf bottom or are transported along the continental slope in a cyclonic direction following the trajectory of the Atlantic waters.

Supplementary Materials: The following are available online at <https://www.mdpi.com/article/10.3390/w16030441/s1>, Table S1: List of experiments on sensitivity to plastic density, particle size and biofouling rate; Figure S1: Simulated microplastic particles distribution after 5 years continued riverine influx without biofouling. (a) HDPE10, (b) HDPE20, (c) PP10, (d) PP20, (e) PS10; Figure S2: Simulated microplastic particles distribution after 5 years continued riverine influx for HDPE with different particle sizes and biofouling rates; Figure S3: Simulated microplastic particles distribution

after 5 years continued riverine influx for PP with different particle sizes and biofouling rates; Figure S4: Simulated microplastic particles distribution after 5 years continued riverine influx for HDPE of the same particle size and biofouling rate with different probability of freezing into ice.

Author Contributions: Conceptualization and methodology, E.G.; software, E.G. and M.G.; validation, E.G. and M.G.; investigation, E.G. and M.G.; writing—original draft preparation, E.G. and M.G.; visualization, M.G. All authors have read and agreed to the published version of the manuscript.

Funding: This research is supported by Russian Science Foundation, Grant 20-11-20112.

Data Availability Statement: The data used in this study are openly available. NCEP/NCAR Reanalysis Data are provided by National Centers for Environmental Prediction/National Weather Service/NOAA/U.S. Department of Commerce. NCEP/NCAR Global Reanalysis Products, 1948–continuing, Research Data Archive <https://psl.noaa.gov/data/gridded/data.ncep.reanalysis.html> (accessed on 1 December 2023). The used version of the ArcticGRO Discharge Dataset and monthly average river discharge temperatures are available online at <https://arcticgreativers.org/discharge/> and <http://research.cfos.uaf.edu/arctic-river/> (the both accessed on 1 December 2023). The model data on microplastic load from rivers to marine waters were published in [26]. Supporting Information are openly available on the American Chemical Society Publications website at <https://doi.org/10.1021/acs.est.7b02368> (accessed on 1 December 2023).

Acknowledgments: The Siberian Branch of the Russian Academy of Sciences (SB RAS) Siberian Supercomputer Center is gratefully acknowledged for providing supercomputer facilities.

Conflicts of Interest: The authors declare no conflict of interest.

References

1. Cózar, A.; Echevarría, F.; González-Gordillo, J.I.; Irigoien, X.; Úbeda, B.; Hernández-León, S.; Duarte, C.M. Plastic debris in the open ocean. *Proc. Nat. Acad. Sci. USA* **2014**, *111*, 10239–10244. [[CrossRef](#)]
2. Andrady, A.L. Persistence of Plastic Litter in the Oceans. In *Marine Anthropogenic Litter*; Bergmann, M., Gutow, L., Klages, M., Eds.; Springer: Cham, Switzerland, 2015. [[CrossRef](#)]
3. Andrady, A.L.; Neal, M.A. Applications and societal benefits of plastics. *Philos. Trans. R. Soc. Lond. B Biol. Sci.* **2009**, *364*, 1977–1984. [[CrossRef](#)]
4. Bergmann, M.; Tekman, M.; Gutow, L. Sea change for plastic pollution. *Nature* **2017**, *544*, 297. [[CrossRef](#)]
5. Bergmann, M.; Allen, S.; Krumpfen, T.; Allen, D. High Levels of Microplastics in the Arctic Sea Ice Alga *Melosira arctica*, a Vector to Ice-Associated and Benthic Food Webs. *Sci. Technol.* **2023**, *57*, 6799–6807. [[CrossRef](#)] [[PubMed](#)]
6. Thushari, G.G.N.; Senevirathna, J.D.M. Plastic pollution in the marine environment. *Heliyon* **2020**, *27*, e04709. [[CrossRef](#)] [[PubMed](#)]
7. Law, K.L. Plastics in the Marine Environment. *Annu. Rev. Mar. Sci.* **2017**, *9*, 205–229. [[CrossRef](#)] [[PubMed](#)]
8. Carbery, M.; O'Connor, W.; Palanisami, T. Trophic transfer of microplastics and mixed contaminants in the marine food web and implications for human health. *Environ. Int.* **2018**, *115*, 400–409. [[CrossRef](#)] [[PubMed](#)]
9. Kühn, S.; Schaafsma, F.L.; van Werven, B.; Flores, H.; Bergmann, M.; Egelkraut-Holtus, M.; van Franeker, J.A. Plastic ingestion by juvenile polar cod (*Boreogadus saida*) in the Arctic Ocean. *Polar Biol.* **2018**, *41*, 1269–1278. [[CrossRef](#)]
10. Tekman, M.B.; Gutow, L.; Macario, A.; Haas, A.; Walter, A.; Bergmann, M. Alfred Wegener Institute Helmholtz Centre for Polar and Marine Research. Litterbase. Available online: <https://litterbase.awi.de/litter> (accessed on 1 December 2023).
11. Kim, S.K.; Lee, H.J.; Kim, J.S.; Kang, S.H.; Yang, E.J.; Cho, K.H.; Tian, Z.; Andrady, A. Importance of seasonal sea ice in the western Arctic ocean to the Arctic and global microplastic budgets. *J. Hazard. Mater.* **2021**, *418*, 125971. [[CrossRef](#)] [[PubMed](#)]
12. Peeken, I.; Primpke, S.; Beyer, B.; Gütermann, J.; Katlein, C.; Krumpfen, T.; Bergmann, M.; Hehemann, L.; Gerdts, G. Arctic sea ice is an important temporal sink and means of transport for microplastic. *Nat. Commun.* **2018**, *9*, 1505. [[CrossRef](#)] [[PubMed](#)]
13. Obbard, R.W.; Sadri, S.; Wong, Y.Q.; Khitun, A.A.; Baker, I.; Thompson, R.C. Global warming releases microplastic legacy frozen in Arctic Sea ice. *Earths Future* **2014**, *2*, 315–320. [[CrossRef](#)]
14. Zhang, Y.; Gao, T.; Kang, S.; Allen, D.; Wang, Z.; Luo, X.; Yang, L.; Chen, J.; Hu, Z.; Chen, P.; et al. Cryosphere as a temporal sink and source of microplastics in the Arctic region. *Geosci. Front.* **2023**, *14*, 101566. [[CrossRef](#)]
15. Yakushev, E.; Gebruk, A.; Osadchiv, A.; Pakhomova, S.; Lusher, A.; Berezina, A.; van Bavel, B.; Vorozheikina, E.; Chernykh, D.; Kolbasova, G.; et al. Microplastics distribution in the Eurasian Arctic is affected by Atlantic waters and Siberian rivers. *Earth Environ.* **2021**, *2*, 23. [[CrossRef](#)]
16. Lusher, A.L.; Tirelli, V.; O'Connor, I.; Officer, R. Microplastics in Arctic polar waters: The first reported values of particles in surface and sub-surface samples. *Sci. Rep.* **2015**, *5*, 14947. [[CrossRef](#)] [[PubMed](#)]
17. Cózar, A.; Martí, E.; Duarte, C.M.; García-de-Lomas, J.; Van Sebille, E.; Ballatore, T.J.; Eguíluz, V.M.; González-Gordillo, J.I.; Pedrotti, M.L.; Echevarría, F.; et al. The Arctic Ocean as a dead end for floating plastics in the North Atlantic branch of the Thermohaline Circulation. *Sci. Adv.* **2017**, *3*, e1600582. [[CrossRef](#)]

18. Kanhai, D.K.; Gårdfeldt, K.; Lyashevskaya, O.; Hassellöv, M.; Thompson, R.C.; O'Connor, I. Microplastics in sub-surface waters of the Arctic Central Basin. *Mar. Pollut. Bull.* **2018**, *130*, 8–18. [[CrossRef](#)]
19. Kanhai, D.K.; Johansson, C.; Frias, J.P.G.L.; Gardfeldt, K.; Thompson, R.C.; O'Connor, I. Deep sea sediments of the Arctic Central Basin: A potential sink for microplastic. *Deep-Sea Res.* **2019**, *145*, 137–142. [[CrossRef](#)]
20. Mu, J.; Qu, L.; Jin, F.; Zhang, S.; Fang, C.; Ma, X.; Zhang, W.; Huo, C.; Cong, Y.; Wang, J. Abundance and distribution of microplastics in the surface sediments from the northern Bering and Chukchi Seas. *Environ. Pollut.* **2019**, *245*, 122–130. [[CrossRef](#)] [[PubMed](#)]
21. Bergmann, M.; Collard, F.; Fabres, J.; Gabrielsen, G.W.; Provencher, J.F.; Rochman, C.M.; van Sebille, E.; Tekman, M.B. Plastic pollution in the Arctic. *Nat. Rev. Earth Environ.* **2022**, *3*, 323–337. [[CrossRef](#)]
22. Allen, D.; Allen, S.; Abbasi, S.; Baker, A.; Bergmann, M.; Brahney, J.; Butler, T.; Duce, R.A.; Eckhardt, S.; Evangelidou, N.; et al. Microplastics and nanoplastics in the marine-atmosphere environment. *Nat. Rev. Earth Environ.* **2022**, *3*, 393–405. [[CrossRef](#)]
23. Mu, J.; Zhang, S.; Qu, L.; Jin, F.; Fang, C.; Ma, X.; Zhang, W.; Wang, J. Microplastics abundance and characteristics in surface waters from the Northwest Pacific, the Bering Sea, and the Chukchi Sea. *Mar. Pollut. Bull.* **2019**, *143*, 58–65. [[CrossRef](#)]
24. Frank, Y.A.; Vorobiev, D.S.; Kayler, O.A.; Vorobiev, E.D.; Kulinicheva, K.S.; Trifonov, A.A.; Hunter, T.S. Evidence for microplastics contamination of the remote tributary of the Yenisey River Siberia—the pilot study results. *Water* **2021**, *13*, 3248. [[CrossRef](#)]
25. Pogojeva, M.; Zhdanov, I.; Berezina, A.; Lapenkov, A.; Kosmach, D.; Osadchiev, A.; Hanke, G.; Semiletov, I.; Yakushev, E. Distribution of floating marine macro-litter in relation to oceanographic characteristics in the Russian Arctic Seas. *Mar. Pollut. Bull.* **2021**, *166*, 112201. [[CrossRef](#)]
26. Schmidt, C.; Krauth, T.; Wagner, S. Export of Plastic Debris by Rivers into the Sea. *Environ. Sci. Technol.* **2017**, *51*, 12246–12253. [[CrossRef](#)] [[PubMed](#)]
27. Van Sebille, E.; Aliani, S.; Law, K.L.; Maximenko, N.; Alsina, J.M.; Bagaev, A.; Bergmann, M.; Chapron, B.; Chubarenko, I.; Cózar, A.; et al. The physical oceanography of the transport of floating marine debris. *Environ. Res. Lett.* **2020**, *15*, 023003. [[CrossRef](#)]
28. Kaiser, D.; Kowalski, N.; Waniek, J.J. Effects of biofouling on the sinking behavior of microplastics. *Environ. Res. Lett.* **2017**, *12*, 124003. [[CrossRef](#)]
29. Morét-Ferguson, S.; Law, K.L.; Proskurowski, G.; Murphy, E.K.; Peacock, E.E.; Reddy, C.M. The size, mass, and composition of plastic debris in the western North Atlantic Ocean. *Mar. Pollut. Bull.* **2010**, *60*, 1873–1878. [[CrossRef](#)] [[PubMed](#)]
30. Chen, X.; Xiong, X.; Jiang, X.; Shi, H.; Wu, C. Sinking of floating plastic debris caused by biofilm development in a freshwater lake. *Chemosphere* **2019**, *222*, 856–864. [[CrossRef](#)] [[PubMed](#)]
31. Fazey, F.M.; Ryan, P.G. Biofouling on buoyant marine plastics: An experimental study into the effect of size on surface longevity. *Environ. Pollut.* **2016**, *210*, 354–360. [[CrossRef](#)] [[PubMed](#)]
32. Geilfus, N.X.; Munson, K.M.; Sousa, J.; Germanov, Y.; Bhugaloo, S.; Babb, D.; Wang, F. Distribution and impacts of microplastic incorporation within sea ice. *Mar. Pollut. Bull.* **2019**, *145*, 463–473. [[CrossRef](#)]
33. Chubarenko, I. Physical processes behind interactions of microplastic particles with natural ice. *Environ. Res. Commun.* **2022**, *4*, 012001. [[CrossRef](#)]
34. Chubarenko, I.; Bocherikova, I.; Esiukova, E.; Isachenko, I.; Kupriyanova, A.; Lobchuk, O.; Fetisov, S. Microplastics in sea ice: A fingerprint of bubble flotation. *Sci. Total. Environ.* **2023**, *892*, 164611. [[CrossRef](#)] [[PubMed](#)]
35. Hoffmann, L.; Eggers, S.L.; Allhusen, E.; Katlein, C.; Peeken, I. Interactions between the ice algae *Fragilariopsis cylindrus* and microplastics in sea ice. *Environ. Int.* **2020**, *139*, 105697. [[CrossRef](#)] [[PubMed](#)]
36. Pradel, A.; Gautier, M.; Bavay, D.; Gigault, J. Micro- and nanoplastics' transfer in freezing saltwater: Implications for their fate in polar waters. *Environ. Sci. Process. Impacts* **2021**, *23*, 1759–1770. [[CrossRef](#)] [[PubMed](#)]
37. Mountford, A.S.; Morales Maqueda, M.A. Eulerian Modeling of the Three-Dimensional Distribution of Seven Popular Microplastic Types in the Global Ocean. *J. Geophys. Res. Oceans* **2019**, *124*, 8558–8573. [[CrossRef](#)]
38. Mountford, A.S.; Morales Maqueda, M.A. Modeling the accumulation and transport of microplastics by sea ice. *J. Geophys. Res. Oceans* **2020**, *126*, e2020JC016826. [[CrossRef](#)]
39. Huserbråten, M.B.; Hattermann, T.; Broms, C.; Albretsen, J. Trans-polar drift-pathways of riverine European microplastic. *Sci. Rep.* **2022**, *12*, 3016. [[CrossRef](#)]
40. Golubeva, E.N.; Platov, G.A. On improving the simulation of Atlantic Water circulation in the Arctic Ocean. *J. Geophys. Res.* **2007**, *112*, C04S05. [[CrossRef](#)]
41. Golubeva, E.N.; Platov, G.A. Numerical modeling of the Arctic Ocean ice system response to variations in the atmospheric circulation from 1948 to 2007. *Izv. Atmos. Ocean. Phys.* **2009**, *45*, 137–151. [[CrossRef](#)]
42. Leonard, B.P. A stable and accurate convective modeling procedure based on quadratic upstream interpolation. *Comput. Methods Appl. Mech. Eng.* **1979**, *19*, 59–98. [[CrossRef](#)]
43. Leonard, B.P.; Lock, A.P.; MacVean, M.K. Conservative explicit unrestricted-timestep multidimensional constancy-preserving advection schemes. *Mon. Weather Rev.* **1996**, *124*, 2588–2606. [[CrossRef](#)]
44. Platov, G.A. Numerical modeling of the Arctic Ocean deepwater formation: Part II. Results of regional and global experiments. *Izv. Atmos. Ocean. Phys.* **2011**, *47*, 377–392. [[CrossRef](#)]
45. Hunke, E.C.; Dukowicz, J.K. An elastic-viscous-plastic model for ice dynamics. *J. Phys. Oceanogr.* **1997**, *27*, 1849–1867. [[CrossRef](#)]
46. Bitz, C.M.; Lipscomb, W.H. An energy-conserving thermodynamic model of sea ice. *J. Geophys. Res.* **1999**, *104*, 15669–15677. [[CrossRef](#)]
47. Lipscomb, W.H.; Hunke, E.C. Modeling Sea Ice Transport Using Incremental Remapping. *Mon. Weather Rev.* **2004**, *132*, 1341–1354. [[CrossRef](#)]

48. Kalnay, E.; Kanamitsu, M.; Kistler, R.; Collins, W.; Deaven, D.; Gandin, L.; Iredell, M.; Saha, S.; White, G.; Woollen, J.; et al. The NCEP/NCAR 40-Year Reanalysis Project. *Bull. Amer. Meteor. Soc.* **1996**, *77*, 437–471. [[CrossRef](#)]
49. Platov, G.A.; Golubeva, E.N.; Kraineva, M.V.; Malakhova V.V. Modeling of climate tendencies in Arctic seas based on atmospheric forcing EOF decomposition. *Oceans Dyn.* **2019**, *69*, 747–767. [[CrossRef](#)]
50. Woodgate, R.A. Increases in the Pacific inflow to the Arctic from 1990 to 2015, and insights into seasonal trends and driving mechanisms from year-round Bering Strait mooring data. *Prog. Oceanogr.* **2018**, *160*, 124–154. [[CrossRef](#)]
51. Vorosmarty, C.J.; Fekete, B.M.; Tucker, B.A. *Global River Discharge, 1807–1991; Version 1.1 (RivDIS)*; ORNL DAAC: Oak Ridge, TN, USA, 1998. [[CrossRef](#)]
52. McClelland, J.W.; Tank, S.E.; Spencer, R.G.M.; Shiklomanov, A.I.; Zolkos S.; Holmes R.M. Arctic Great Rivers Observatory. Discharge Dataset, Version 20230810. 2023. Available online: <https://arcticgreatrivers.org/discharge/> (accessed on 1 December 2023).
53. Whitefield, J.; Winsor, P.; McClell, J.; Menemenlis, D. A new river discharge and river temperature climatology data set for the pan-Arctic region. *Oceans Model.* **2015**, *88*, 1–15. [[CrossRef](#)]
54. Forum for Arctic Modeling and Observational Synthesis. Available online: <https://web.whoi.edu/famos> (accessed on 1 December 2023).
55. Proshutinsky, A.; Aksenov, Y.; Clement Kinney, J.; Gerdes, R.; Golubeva, E.; Holland, D.; Holloway, G.; Jahn, A.; Johnson, M.; Popova, E.; et al. Recent advances in Arctic ocean studies employing models from the Arctic Ocean Model Intercomparison Project. *Oceanography* **2011**, *24*, 102–113. [[CrossRef](#)]
56. Proshutinsky, A.; Krishfield, R.; Toole, J.M.; Timmermans, M.L.; Williams, W.; Zimmermann, S.; Yamamoto-Kawai, M.; Armitage, T.W.K.; Dukhovskoy, D.; Golubeva, E.; et al. Analysis of the Beaufort Gyre freshwater content in 2003–2018. *J. Geophys. Res. Oceans* **2019**, *124*, 9658–9689. [[CrossRef](#)]
57. Aksenov, Y.; Karcher, M.; Proshutinsky, A.; Gerdes, R.; de Cuevas, B.; Golubeva, E.; Kauker, F.; Nguyen, A.T.; Platov, G.A.; Wadley, M.; et al. Arctic pathways of Pacific Water: Arctic Ocean Model Intercomparison experiments. *J. Geophys. Res. Oceans* **2016**, *121*, 27–59. [[CrossRef](#)] [[PubMed](#)]
58. Platov, G.A.; Golubeva, E.N. Interaction of Dense Shelf Waters of the Barents and Kara Seas with the Eddy Structures. *Phys. Oceanogr.* **2019**, *26*, 484–503. [[CrossRef](#)]
59. Golubeva, E.; Kraineva, M.; Platov, G.; Iakshina, D.; Tarkhanova, M. Marine heatwave in Siberian Arctic Seas and adjacent region. *Remote Sens.* **2021**, *13*, 4436. [[CrossRef](#)]
60. Malakhova, V.; Golubeva, E. Model Study of the Effects of Climate Change on the Methane Emissions on the Arctic Shelves. *Atmosphere* **2022**, *13*, 274. [[CrossRef](#)]
61. Gradova, M.A.; Golubeva, E.N. Evaluation of the Riverine Heat Influx Impact on the Arctic Ice Cover Based on Numerical Modeling. *Russ. Meteorol. Hydrol.* **2023**, *48*, 639–644. [[CrossRef](#)]
62. Zhiyao, S.; Tingting, W.; Fumin, X.; Ruijie, L. A simple formula for predicting settling velocity of sediment particles. *Water Sci. Eng.* **2008**, *1*, 37–43. [[CrossRef](#)]
63. Chubarenko, I.; Bagaev, A.; Zobkov, M.; Esiukova, E. On some physical and dynamical properties of microplastic particles in marine environment. *Mar. Pollut. Bull.* **2016**, *108*, 105–112. [[CrossRef](#)] [[PubMed](#)]
64. Fisher, N.S.; Bjerregaard, P.; Fowler, S.W. Interactions of marine plankton with transuranic elements. 1. Biokinetics of neptunium, plutonium, americium, and californium in phytoplankton. *Limnol. Oceanogr.* **1983**, *28*, 432–447. [[CrossRef](#)]
65. Wassmann, P.; Reigstad, M. Future Arctic Ocean seasonal ice zones and implications for pelagic-benthic coupling. *Oceanography* **2011**, *24*, 220–231. [[CrossRef](#)]
66. Kanhai, L.D.K.; Gardfeldt, K.; Krumpfen, T.; Thompson, R.C.; O’Connor, I. Microplastics in sea ice and seawater beneath ice floes from the Arctic Ocean. *Sci. Rep.* **2020**, *10*, 5004. [[CrossRef](#)] [[PubMed](#)]
67. Jalón-Rojas, I.; Wang, X.H.; Fredj, E. A 3D numerical model to Track Marine Plastic Debris (TrackMPD): Sensitivity of microplastic trajectories and fates to particle dynamical properties and physical processes. *Mar. Pollut. Bull.* **2019**, *141*, 256–272. [[CrossRef](#)] [[PubMed](#)]
68. Korsnes, R.; Pavlova, O.; Godtlielsen, F. Assessment of potential transport of pollutants into the Barents Sea via sea ice—An observational approach. *Mar. Pollut. Bull.* **2002**, *44*, 861–869. [[CrossRef](#)] [[PubMed](#)]
69. Emberson-Marl, H.R.L.; Coppock, M.; Cole, B.J.; Godley, N.; Mimpriss, S.E.; Nelms, P.K.; Lindeque, P.K. Microplastics in the Arctic: A transect through the Barents Sea. *Front. Mar. Sci. Sec. Mar. Pollut.* **2023**, *10*, 1241829. [[CrossRef](#)]
70. Kooi, M.; van Nes, E.H.; Scheffer, M.; Koelmans, A.A. Ups and downs in the ocean: Effects of Biofouling on Vertical Transport of Microplastics. *Environ. Sci. Technol.* **2017**, *51*, 7963–7971. [[CrossRef](#)]
71. Gilfillan, L.R.; Ohman, M.D.; Doyle, M.J.; Watson, W. Occurrence of plastic micro-debris in the Southern California Current System. *CalCOFI Rep.* **2009**, *50*, 123–133.
72. Xiao, S.; Cui, Y.; Brahney, J.; Mahowald, N.M.; Li, Q. Long-distance atmospheric transport of microplastic fibres influenced by their shapes. *Nat. Geosci.* **2023**, *16*, 863–870. [[CrossRef](#)]

Disclaimer/Publisher’s Note: The statements, opinions and data contained in all publications are solely those of the individual author(s) and contributor(s) and not of MDPI and/or the editor(s). MDPI and/or the editor(s) disclaim responsibility for any injury to people or property resulting from any ideas, methods, instructions or products referred to in the content.